Rejection of Electronic Recoils with the DMTPC Dark Matter Search

Available online at www.sciencedirect.com

SciVerse ScienceDirect

Physics Procedia 37 (2012) 575 – 582

Physics Procedia

TIPP 2011 - Technology and Instrumentation for Particle Physics 2011

Rejection of Electronic Recoils with the DMTPC Dark Matter Search

J.P. Lopez[a], S. Ahlen[b], J. Battat[c], T. Caldwell[a], M. Chernicoff[b], C. Deaconu[a], D. Dujmic[d,a], A. Dushkin[e], W. Fedus[a], P. Fisher[d,a,f], F. Golub[e], S. Henderson[a], A. Inglis[b], A. Kaboth[a], G. Kohse[g], L. Kirsch[e], R. Lanza[g], A. Lee[a], J. Monroe[h,a], H. Ouyang[e], T. Sahin[a], G. Sciolla[e], N. Skvorodnev[e], H. Tomita[b], H. Wellenstein[e], I. Wolfe[a], R. Yamamoto[a], H. Yegoryan[a]

[a]*Physics Department, Massachusetts Institute of Technology; Cambridge, MA 02139, USA*
[b]*Physics Department, Boston University; Boston, MA 02215, USA*
[c]*Physics Department, Bryn Mawr College; Bryn Mawr, PA 19010, USA*
[d]*Laboratory for Nuclear Science, Massachusetts Institute of Technology; Cambridge, MA 02139, USA*
[e]*Physics Department, Brandeis University; Waltham, MA 02453, USA*
[f]*MIT Kavli Institute for Astrophysics and Space Research, Massachusetts Institute of Technology; Cambridge, MA 02139, USA*
[g]*Nuclear Science and Engineering Department, Massachusetts Institute of Technology; Cambridge, MA 02139, USA*
[h]*Physics Department, Royal Holloway, University of London; Egham, TW20 0EX, UK*

Abstract

The Dark Matter Time Projection Chamber (DMTPC) collaboration is developing a low-pressure gas TPC for detecting WIMP-nucleon interactions. DMTPC detectors use optical readout with CCD cameras to search for the daily modulation of the directional signal of the dark matter wind. An analysis of several charge readout channels has been developed to obtain additional information about ionization events in the detector. In order to reach sensitivities required for the WIMP detection, the detector needs to minimize backgrounds from electron recoils. This article shows that by using the readout of charge signals in addition to CCD readout, a preliminary statistics-limited 90% C.L. upper limit on the γ and e^- rejection factor of 5.6×10^{-6} is obtained for energies between 40 $\mathrm{keV_{ee}}$ and 200 $\mathrm{keV_{ee}}$.

Keywords: Dark matter, TPC, WIMP, Dark matter wind, Direct detection

1. Introduction

The DMTPC collaboration uses a low-pressure time projection chamber (TPC) with directional sensitivity to search for interactions between weakly-interacting massive particles (WIMPs) and nucleons from WIMPs in the galactic dark matter halo. These elastic scattering events create low-momentum nuclear recoils that leave ionization trails inside the detector. In the 75 Torr CF_4 gas used as a target material, these are roughly 1 to 2 mm in length. DMTPC detectors achieve sub-millimeter pixelation of the TPC readout plane

Email address: jplopez@mit.edu (J.P. Lopez)

1875-3892 © 2012 Published by Elsevier B.V. Selection and/or peer review under responsibility of the organizing committee for TIPP 11.
doi:10.1016/j.phpro.2012.03.716

using charge-coupled device (CCD) cameras and are able to reconstruct the angular distribution of nuclear recoils [1]. Additional information about ionization events is obtained with several charge-readout channels. The expected angular distribution of the galactic WIMP wind is distinct from all known backgrounds and allows a statistical test of whether a potential signal is from WIMPs or backgrounds [2, 3, 4, 5, 6, 7].

Electronic recoils from nuclear decays due to radioactive material in the detector and in the laboratory environment are typically one of the most important backgrounds for dark matter searches. Gas TPCs are ideal detectors for differentiating electrons from nuclear recoils because in a low-density detector medium electronic recoils have much longer ranges than nuclear recoils and αs of the same energy. This article describes the ability of DMTPC detectors to reject these types of events.

2. Detector Design

The data set described in this article was taken in a surface laboratory in Cambridge, Massachusetts using a prototype DMTPC detector, shown in Fig. 1. A schematic of the detector design is given in Fig. 2. The TPC consists of a field cage with a 10 cm drift length with a cathode wire mesh held at -1.2 kV at one end and a wire mesh held at ground at the other [1]. Copper rings with an inner radius of 27 cm shape the field and define the boundary of the field cage. An amplification gap is created by separating the grounded mesh from an anode plate of copper-clad G10 with 440 μm diameter dielectric wires. The anode plate is held at 680 V. The TPC is placed inside a vacuum vessel filled with 75 Torr CF_4 gas.

Fig. 1. Picture of the detector used in this analysis. The TPC is held within the cylindrical vacuum vessel. The CCD is the blue box on top of the vacuum vessel. The lens and the vessel viewport are not visible.

The light signals from the amplification region are measured by an Apogee Alta U6 CCD camera, which uses a Kodak KAF-1001 1024 by 1024 pixel CCD chip. The 24 μm by 24 μm pixels are read out in 4 by 4 blocks, resulting in a 256 bin by 256 bin image. A lens directs the light from a 16.7 cm by 16.7 cm section at the center of the anode onto the CCD, so each bin in the image corresponds to a 650 μm by 650 μm square region of the anode. The energy response of the CCD is calibrated by placing a 4.44 ± 0.04 MeV ^{241}Am source [8] inside the field cage. The CCD measures the full α energy, and the mean energy is compared to the known calibrated value to obtain a calibration of 13.1 ± 0.1 analog-to-digital units (ADU) per keV of deposited energy. Stopping power predictions from SRIM [9] show that almost all the energy loss of the αs is due to ionization, so the measured α energy is approximately equal to electron-equivalent ionization energy loss at the same energy, if radiation is ignored. Measured energies are reported in ^{241}Am α-equivalent units, denoted $\mathrm{keV_{ee}}$.

The anode plate is separated into two active regions, the outer 1 cm of the 26.7 cm field cage (veto region) and an inner region (anode region) to measure signal events. The signals from the veto region are fed into a Cremat CR-112 charge-sensitive preamplifier (CSP) and are used to identify events that are not

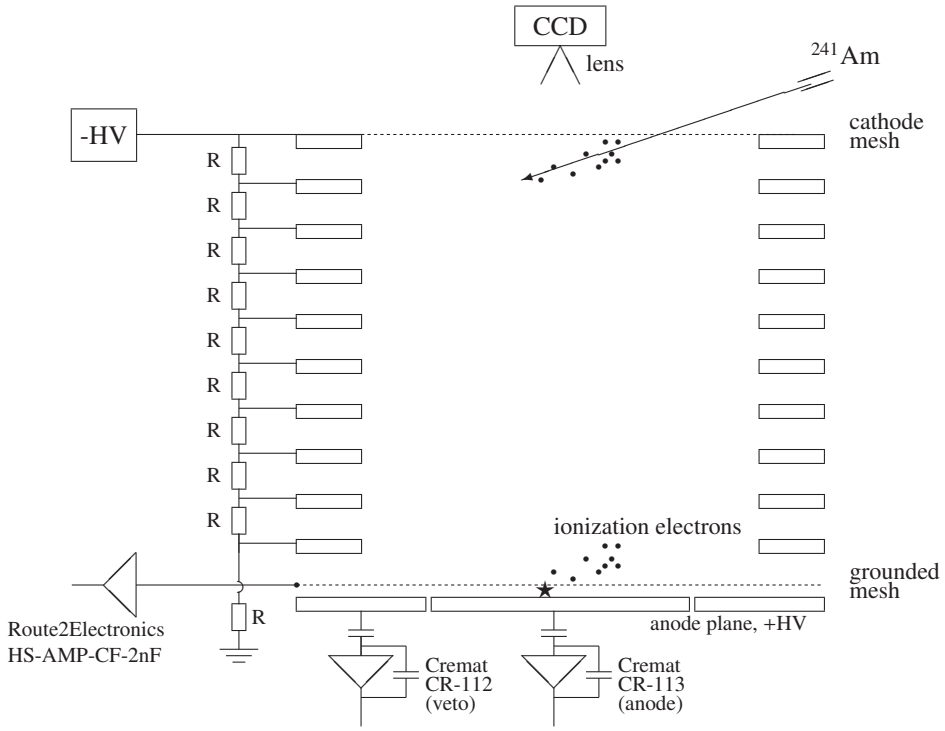

Fig. 2. A schematic of the detector: the drift field is created by a cathode mesh, field-shaping rings attached to a resistor chain and a ground mesh. Primary ionization from a recoiling nucleus is drifted down to the ground mesh. The high-field amplification region is formed by the ground mesh and the anode plane. The ground mesh is read out with a fast amplifier and the veto and anode are readout with charge-sensitive preamplifiers. Scintillation light from the amplification region is recorded with the CCD camera.

fully contained within the field cage. The signals from the anode region are fed into a Cremat CR-113 CSP and are used to obtain a measurement of the recoil energy and the time of the recoil. The CR-112 has a gain of 15 mV/pC while that of the CR-113 is 1.5 mV/pC. When unconnected to the detector, the CSPs have a rise time of 20 ns and an exponential decay constant of 50 μs.

The current signal from the grounded mesh is fed into a Route2Electronics HS-AMP-CF amplifier, with a gain of 80 and a rise time of approximately 1 ns. The signal of an electron avalanche has two parts. The first is the signal from the electrons in the avalanche. Most of the ionization occurs very near the anode, so a sharply rising current signal is seen that decays in less than 1 ns. The second part of the signal is from the ions drifting toward the grounded mesh. These drift much slower and on average over a longer distance than the electrons, so the current is smaller than for electrons but the integrated charge is greater. In the drift region of the detector, nuclear recoils leave a compact ionization trail. The recoil range along the drift direction (Δz) is no more than a few millimeters. The time spread due to Δz, determined by the electron drift velocity, is $\Delta z \times 10$ ns/mm [10], so the electrons all reach the amplification region within a period of a few times 10 ns. Electronic recoils and minimum ionizing particles have much larger typical Δz than nuclear recoils of similar energy, often several centimeters or more. With such a long Δz, the electron and ion signals of the avalanches merge, leaving a current signal with a single peak that is smaller than that seen for nuclear recoils and with a much longer rise time. Example signals of a low-energy α, similar to a nuclear recoil, and an electronic recoil are shown in Figs. 3 and 4 .

The charge channels are digitized by AlazarTech ATS860 8-bit PCI digitizers with a 250 MHz sampling rate. The digitizer is triggered from either the mesh or central anode channel, with the trigger level set to obtain high efficiency for $E > 30$ keV$_{ee}$. Each waveform consists of 4096 (16.4 μs) pre-trigger samples and 8192 (32.8 μs) post-trigger samples to allow for pulse shape analysis. During readout, the CCD is exposed

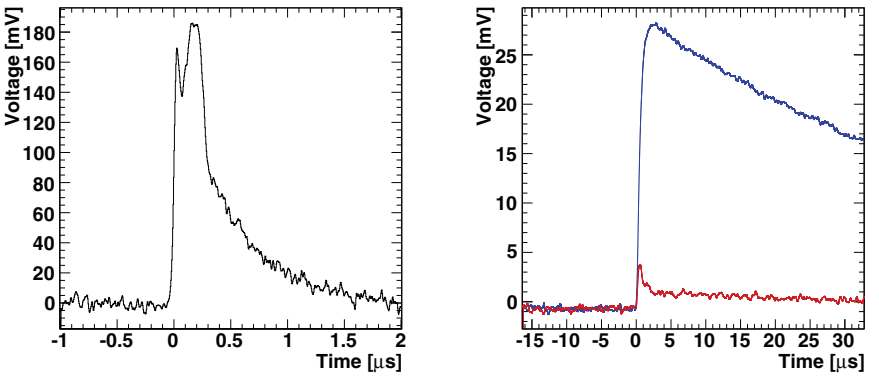

Fig. 3. Example charge signals from a 113 keV$_{ee}$ α particle. Left: Mesh (current) signal. Note the two-peaked shape of the pulse, characteristic of nuclear recoils and similar events. Right: Anode (blue) and veto (red) signals.

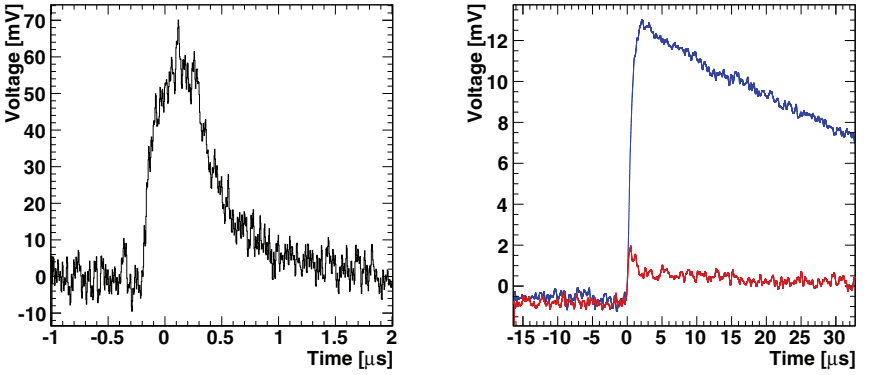

Fig. 4. Example charge signals from a 54 keV$_{ee}$ electronic recoil. Left: Mesh (current) signal. Only one broad peak is seen here in the mesh signal. Right: Anode (blue) and veto (red) signals. The small size and fast rise time of the veto pulse shape are characteristic of a crosstalk signal rather than ionization in the veto region.

for 1 s while the charge channels are concurrently collecting data. After each exposure, the image and any charge triggers are written to file for processing and analysis.

3. Event Reconstruction

3.1. CCD Tracks

The reconstruction of recoil events in the CCD readout is described in [11]. The energy, projected two-dimensional range and several moments of a recoil are measured from the CCD image. The analysis in this article uses a simpler set of selection cuts than were used in [11] in order to increase the efficiency of the CCD reconstruction for nuclear recoils. CCD-related artifacts such as interactions in the CCD chip and hot pixels are identified and removed by restricting the maximum amount of charge measured in any pixel, by requiring that no single pixel contain more than 25% of the light signal of the recoil, and by requiring that the peak pixel values be high enough to determine the recoil range. Events reaching the edge of the CCD image and multiple potential recoils occurring less than 10 pixels apart within 1000 one-second exposures are rejected. From Monte Carlo studies, the reconstruction and cuts are expected to reach > 90% efficiency for ionization yields of E>40 keV$_{ee}$.

3.2. Anode and Veto Signals

The anode and veto channel signals are first smoothed using a Gaussian convolution with $\sigma = 80$ ns to reduce the noise. The width of the Gaussian is much smaller than the size of features in nuclear recoil signals and will not significantly change the measured parameters from their true values. The pre-trigger region is then used to determine the baseline mean and standard deviation for each trace. The peak value of the smoothed pulse and the time at which the peak occurs are recorded. The baseline crossings closest to the peak in either direction in time are determined. From these crossings, the times where the signal first reaches 10%, 25%, 50%, 75% and 90% of the peak height are recorded to obtain information about the pulse shape. The pulse shape of the anode signal is used to identify and possible noise events. The pulse shape of the veto signal is used to differentiate a crosstalk signal from the anode from a true signal from ionization occurring in the veto region.

3.3. Mesh Signals

The time scales of the features in the current signals read from the mesh channel are much faster than those in the other channels, so a Gaussian convolution with $\sigma = 6$ ns is used to reduce the noise. Again, this is shorter than the scale of the features measured in this data set and does not significantly alter the values obtained from their true values. As with the other channels, the baseline, pulse peak value and time, and several times along the rising and falling edges are recorded.

Additional information about the mesh signal electron and ion peaks are recorded as well. The electron peak is identified with the first peak in the pulse with a height greater than 50% of the pulse maximum value. The ion peak is identified with the highest peak in the pulse occurring more than 50 ns after the electron peak. The times and heights of these peaks and the minimum point between them are recorded. Several times along the rising edge between the initial baseline crossing and the electron peak are recorded. Similar values are calculated along the falling edge after the ion peak. Finally, the pulse integral, proportional to the track energy, is calculated.

3.4. Selection Cuts for Nuclear Recoils

To determine selection criteria for nuclear recoils, a ^{241}Am α source was placed above the cathode mesh so that only a small part of the tracks entered the active volume of the detector. This is shown in the schematic in Fig. 2. With this setup, α particles are measured with energies ranging from a few tens to a few hundred keV. The primary ionization electrons drift across the full 10 cm drift length. Three sets of cuts are used to suppress background evets: (1) removal of electronic noise and pulses only partially contained in the saved traces; (2) removal of recoils passing over or through the veto region; and (3) removal of electronic recoil events that pass the cuts in (2).

The noise reduction cuts remove events with baseline properties and pulse rise and fall times deviating from the expected range. The analysis ensures that the full mesh pulse is included in the saved waveforms and that the mesh and anode pulses are properly correlated in time. Events where one of the channels reaches the maximum input value of the digitizer are removed as well.

Events where the peak voltage of the veto channel is greater than 25% of the anode channel peak value are considered to have passed over the veto region and are rejected. Recoils above the central anode region typically create an induced crosstalk signal on the veto channel. These crosstalk signals have sharper rise and fall times compared to the signal pulses from electron avalanches in the veto region. Events where the veto channel has a 25% peak to 90% peak rise time greater than 400 ns have the characteristic shape of a signal pulse and are rejected. Finally, events where the veto channel pulse and mesh channel pulse are not well-correlated, due to event pileup in the veto channel are also removed as they will likely be poorly reconstructed. Such events are rare in running without sources.

Electronic recoils are identified and rejected using the shape of the mesh signal. As described in Section 2, nuclear recoils are expected to have shorter rise times and higher, sharper peak values compared to electronic recoils of the same energy. For nuclear recoils, the 25% peak to 75% peak rise time of the electron peak must be less than 22 ns for energies less than 140 keV_{ee} (Fig. 5). The ratios of the mesh electron and ion peak heights (V_{electron} and V_{ion}) compared to the anode channel peak height V_{anode} provide

additional shape parameters. For nuclear recoils must have $V_{\text{electron}}/V_{\text{anode}} > 4.5$ and $V_{\text{electron}}/V_{\text{anode}} > 5.5$ (Fig. 6). These cut values are determined from the low-energy α calibration data. Due to the high diffusion and longer ranges of the α tracks in that data compared to nuclear recoils, the cuts will still be valid for both fluorine and carbon recoils.

Applying these cuts gives us a set of CCD and charge signals from potential nuclear recoils. The next step is to match the CCD signal to the corresponding charge signal. This is done because when using the α source there are often several tracks in a single image. The matching algorithm examines all possible pairs of charge and CCD signals and chooses the best matches according to the calibration $E_{\text{anode}}[\text{mV}] = (3.07 \pm 0.04) + (0.01916 \pm 0.00002)E_{\text{CCD}}[\text{ADU}]$, obtained using the ^{241}Am α data. Events are accepted if the measured anode energy differs from the best fit value calculated from the CCD energy by less than 8.5 mV (Fig. 7).

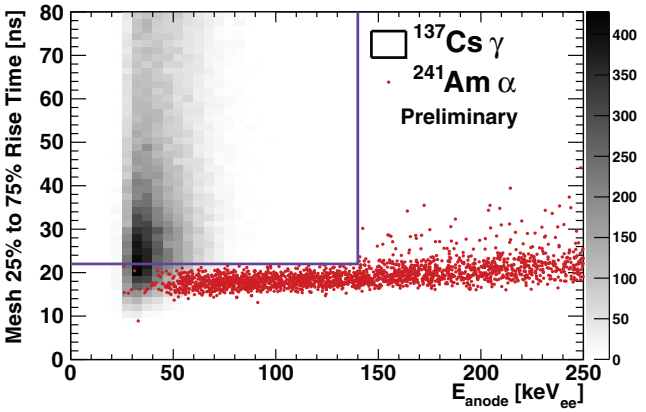

Fig. 5. Energy (keV_{ee}) vs mesh channel 25% to 75% rise time (ns). Red: Low-energy α particles passing all cuts. Histogram: ^{137}Cs γ charge signals passing noise and veto cuts. The violet lines show the rise time cut region for selecting α particles and nuclear recoils.

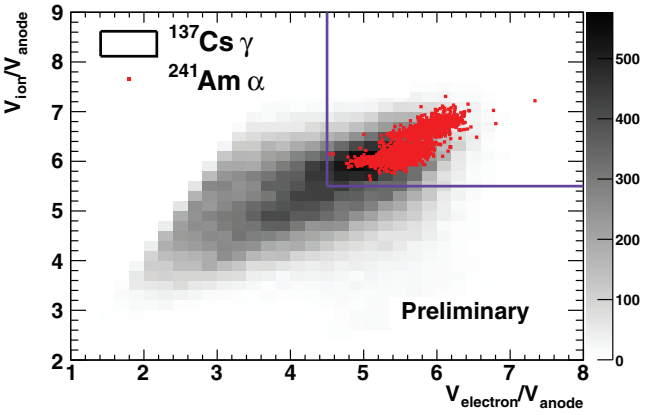

Fig. 6. Ratio of mesh electron peak and anode peak height vs ratio of mesh ion peak height and anode peak height. Red: Low energy α particles passing all cuts. Histogram: ^{137}Cs γ charge signals passing noise and veto cuts. The violet lines show the peak ratio cut region for selecting α particles and nuclear recoils. These variables parameterize the mesh signal width.

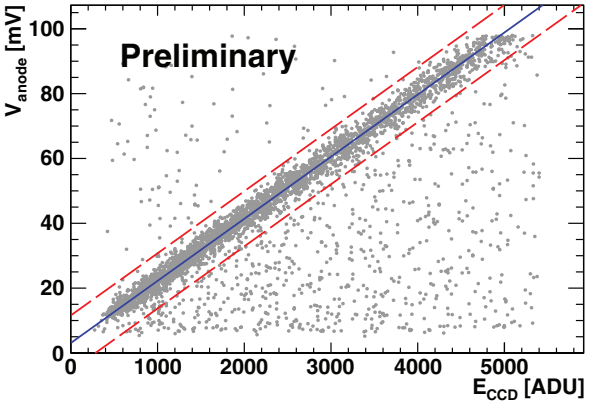

Fig. 7. CCD light energy (ADU) vs anode charge energy. Points: Low energy α data passing all cuts. Blue: Best fit line to band of matching charge-light signals. Red: Boundaries of region for accepting good charge-light matches. The red lines are 8.5 mV from the best fit line.

4. Results

The goal of this analysis is to measure the number of electronic recoils in the sensitive volume of the detector using the charge readout signals, and then apply the electron rejection cuts to measure the rejection capability of the detector. To generate electronic recoils, a 5 μCi collimated ^{137}Cs γ source was deployed inside the detector. The 660 keV gammas generate Compton-scattering-induced electronic recoils throughout the detector with energies similar to those of interest for WIMP searches. While the individual recoils are not typically measured in the CCD, the distribution of light from ionization created by the source is measured using the average of several thousand CCD exposures. This distribution is used to determine that 68% of the recoils occur in the region read out by the CCD camera.

On average 27 valid charge events passing the noise cuts in each 1 s exposure in the ^{137}Cs run with energies between 40 and 200 keV$_{ee}$. The energy spectrum of the source and the estimated background spectrum is shown in Fig. 8. The CCD accumulates all light signals during the exposure. At this event rate, the overlap of several electronic recoils can be misidentified as a nuclear recoil. This results in a set of background events that will not be seen in WIMP searches, where the rate of electronic recoils is much lower. After removing events where a spark occurred on the anode, the ^{137}Cs run contained a total exposure of 14.18 hours. After applying the noise rejection cuts, 679939 charge events are measured with 40 keV$_{ee}$ $< E_{\mathrm{anode}} <$ 200 keV$_{ee}$. Of these, 255 pass the veto and electronic recoil rejection cuts and only 5 have a matching signal in the CCD data.

A separate run was taken with no sources inside the chamber to compare to the ^{137}Cs data. This run had a total exposure time of 9.05 hours. In this data, 49339 events with 40 keV$_{ee}$ $< E_{\mathrm{anode}} <$ 200 keV$_{ee}$ pass the noise rejection cuts with 35 passing the veto and electronic recoil rejection cuts. Three events have a matching signal in the CCD data.

Combining the results of the ^{137}Cs run and the source-free run, the source generated 602600 ± 350(stat) recoil events with 40 keV$_{ee}$ $< E <$ 200 keV$_{ee}$ inside the drift region of the detector, 68% of which were in the region viewed by the CCD. A charge-only analysis yields 200 ± 9 electronic recoils passing the cuts, resulting in a rejection power of $(3.32 \pm 0.15) \times 10^{-4}$ for the charge analysis. Considering the full analysis by requiring coincident charge and light signals, 5 events are measured in the ^{137}Cs data with an estimated background of 4.7 ± 2.7 events. The recoil ranges and peak CCD pixel values are more consistent with nuclear recoils than what is expected for electronic recoils, so these can be rejected as electronic recoil candidates. With no recoil candidates, a 90% C.L. upper limit on the electronic recoil rejection power from the full CCD and charge combined analysis of 5.6×10^{-6} for 40 keV$_{ee}$ $< E <$ 200 keV$_{ee}$.

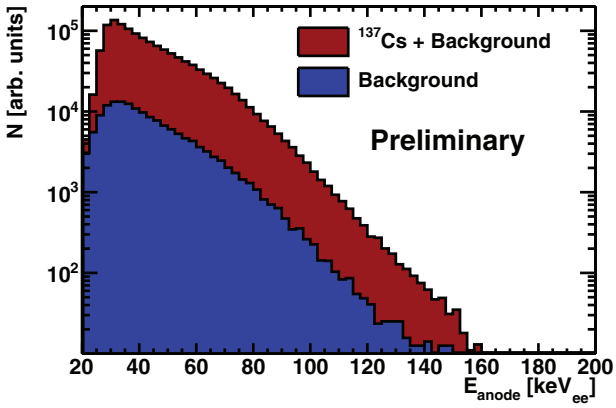

Fig. 8. Red: Energy spectrum of the ^{137}Cs source, including background. Blue: Estimated background spectrum measured in source-free run.

5. Conclusions

This work demonstrates the ability of a DMTPC detector to reject electronic recoils at the level of 5.6×10^{-6} at 90% C.L. for 40 $keV_{ee} < E < 200$ keV_{ee}. This is a conservative limit due to the large number of recoils in each CCD exposure compared to background level. The charge analysis alone has an electronic recoil rejection factor of $(3.32 \pm 0.15) \times 10^{-4}$. The charge readout enhances the capabilities of DMTPC detectors to reject these backgrounds compared to previous CCD-only analyses backgrounds. The charge readout channels have been deployed on DMTPC detectors designed for underground running and will be used in future WIMP searches.

Acknowledgements

The DMTPC collaboration would like to acknowledge support by the U.S. Department of Energy (grant number DE-FG02-05ER41360), the Advanced Detector Research Program of the U.S. Department of Energy (contract number 6916448), as well as the Reed Award Program, the Ferry Fund, the Pappalardo Fellowship program, the MIT Kavli Institute for Astrophysics and Space Research, the MIT Bates Research and Engineering Center, and the Physics Department at the Massachusetts Institute of Technology. We would like to thank Mike Grossman for valuable technical assistance.

References

[1] D. Dujmic, et al., Charge amplification concepts for direction-sensitive dark matter detectors, Astropart. Phys. 30 (2008) 58–64.
[2] S. Ahlen, et al., The case for a directional dark matter detector and the status of current experimental efforts, Int. J. Mod. Phys. A25 (2010) 1–51.
[3] D. Spergel, Motion of the Earth and the detection of weakly interacting massive particles, Phys. Rev. D 37 (1988) 1353–1355.
[4] J. Lewin, P. Smith, Review of mathematics, numerical factors, and corrections for dark matter experiments based on elastic nuclear recoil, Astropart. Phys. 6 (1996) 87–112.
[5] A. M. Green, B. Morgan, Optimizing WIMP directional detectors, Astropart. Phys. 27 (2007) 142–149.
[6] B. Morgan, A. M. Green, Directional Statistics for WIMP direct detection II: 2-d read-out, Phys. Rev. D72 (2005) 123501.
[7] B. Morgan, A. M. Green, N. J. C. Spooner, Directional statistics for WIMP direct detection, Phys. Rev. D71 (2005) 103507.
[8] H. Yegoryan, Study of Alpha Background in a Dark Matter Detector, Senior Thesis, Massachusetts Institute of Technology.
[9] J. Ziegler, J. Biersack, U. Littmark, Pergamon Press, New York, 1985, http://www.srim.org/.
[10] L. Christophorou, et al., Electron Interactions with CF_4, J. Phys. Chem. Re. Data. 25 (1996) 1341–1388.
[11] S. Ahlen, et al., First Dark Matter Search Results from a Surface Run of the 10-L DMTPC Directional Dark Matter Detector, Phys. Lett. B695 (2011) 124–129.